$N^{14}+He^4$ and $O^{16}+He^3$ Differential Cross Sections*

E. A. SILVERSTEIN,† S. R. SALISBURY, G. HARDIE, AND L. D. OPPLIGER
University of Wisconsin, Madison, Wisconsin

(Received June 22, 1961)

Thin (~2 kev) gas targets have been used for high-resolution studies of $N^{14}(\alpha,\alpha)N^{14}$ differential cross sections for $1.0<E_\alpha<2.4$ Mev. Data were taken at five angles. Resonances were observed at $E_\alpha=1.533$, 1.620, 2.165, 2.351, and 2.370 Mev. The Wigner-Eisenbud formalism was used to extract resonant parameters (where possible) of the corresponding virtual states of F^{18}. Also $O^{16}(He^3,He^3)O^{16}$ and $O^{16}(He^3,He^4)O^{15}$ differential cross sections were measured for $1<E_{He^3}<3$ Mev. A 300-kev broad resonance at $E_{He^3}=2.360$ Mev was shown to result from a $\frac{1}{2}^+$ state of Ne^{19}. The elastic width is 0.11 of the total width.

I. INTRODUCTION

ELASTIC scattering is a useful tool for the study of virtual energy levels of the resultant compound nucleus. The scattering is described in terms of parameters associated with the energy levels of the compound nucleus formed from the incident particle and the target nucleus. These level parameters are the energy of the virtual state E_λ, the angular momentum and parity J^π, a reduced width $\gamma_{\lambda s}^2$ and an interaction radius a_s for each channel, and the isobaric spin T. By use of the Wigner-Eisenbud one-level formula these parameters often can be assigned from the cross-section data. A general discussion of experimental techniques and interpretation of the data in gas scattering experiments appear in Richard's article.[1]

The present low-energy $N^{14}(\alpha,\alpha)N^{14}$ elastic scattering work was undertaken to study levels in F^{18} at $E_\alpha=1.53$ and 1.62 Mev seen in $N^{14}(\alpha,\gamma)F^{18}$ work by Price[2] and Phillips[3] and to study other F^{18} levels in this energy region seen by Hinds and Middleton[4] in the $F^{19}(He^3,\alpha)F^{18}$ reaction.

The recent availability of low-cost He^3 ($0.15 per cc) permits its use in rf ion sources without provision for recovery. Hence a study of Ne^{19} levels by $O^{16}(He^3,He^3)O^{16}$ elastic scattering was feasible. The excitation energy ($E_x=8.42$ Mev) of the compound nucleus Ne^{19} formed by $O^{16}+He^3$ is low enough so that one expects to find well-separated levels. The He^3 studies were terminated before background difficulties were eliminated. This termination resulted from an unexpected policy reversal by the He^3 supplier regarding the availability of He^3. Hence, the He^3 data presented here are not as complete or accurate as might be desired.

II. EXPERIMENTAL ARRANGEMENT

The α-particle and He^3 beams were obtained from the University of Wisconsin 4-Mev electrostatic generator. The beams were momentum analyzed by a 15° magnetic analyzer, and then energy analyzed by a 90° electrostatic analyzer set for an energy resolution of about 0.06%.

The gas scattering chamber used is shown in Fig. 1. The steel chamber has a volume of about 0.7 liter. The rotating seals are double with a pump-out between. The counter moves in a cone making an angle of 14° with the horizontal. Hence, the laboratory scattering angle varies from 14° to 166° as the top is rotated. The differential pumping system and the counter system are connected to the chamber body by flexible couplings, allowing adjustment for alignment.

The number of counts Y is given in terms of the differential cross section σ by

$$Y=nNG/\sin\theta_{\text{lab}}, \quad (1)$$

where n is the number of target nuclei per cm^3, N is the number of bombarding particles per data run, and G is the G factor of the counter system—corresponding to a solid angle. The counter system uses circular front and rear apertures. Expressions for the G factor of such systems are given by Silverstein.[5] By use of such an aperture system it is possible to eliminate the usual rotating joint necessary to keep a rectangular-front aperture perpendicular to the scattering plane.

The differential pumping system consists of three sets of impedances with pumping between the first and second and between the second and third. The first pumping stage consists of a Heraeus-Roots pump VP-R-150E (40 liters per second at $p\approx10^{-2}$ mm Hg), backed by a Kinney pump No. CVD556 (≈5 liters per second from 10^{-3} to 1 mm Hg). The second pumping stage consists of a Consolidated VMF 260 diffusion pump. The differential pumping impedances are made of 0.1-mm thick stainless steel with a 2-mm diam hole. The system can easily handle a chamber pressure of 25 mm Hg with oxygen used as a target gas.

The vacuum in the collector cup (Fig. 1) is maintained at around 10^{-6} mm Hg by a diffusion pump. The cup is isolated from the chamber by a nickel foil—thicknesses ranging from 750 to 2500 A were used. The foils were first mounted onto a stainless steel ring which was then fastened to the cup by studs protruding from the

* Work supported in part by the U. S. Atomic Energy Commission and by the Graduate School from funds supplied by the Wisconsin Alumni Research Foundation.

† Now at University of Padua, Padua, Italy.

[1] H. T. Richard, in *Nuclear Spectroscopy*, edited by Fay Ajzenberg-Selove (Academic Press, Inc., New York, 1960), Part A, I–D.

[2] P. C. Price, Proc. Phys. Soc. (London) **A68**, 553 (1955).

[3] W. R. Phillips, Phys. Rev. **110**, 1408 (1958).

[4] S. Hinds and R. Middleton, Proc. Phys. Soc. (London) **A73**, 721 (1959).

[5] E. A. Silverstein, Nuclear Instr. and Methods **4**, 53 (1959).

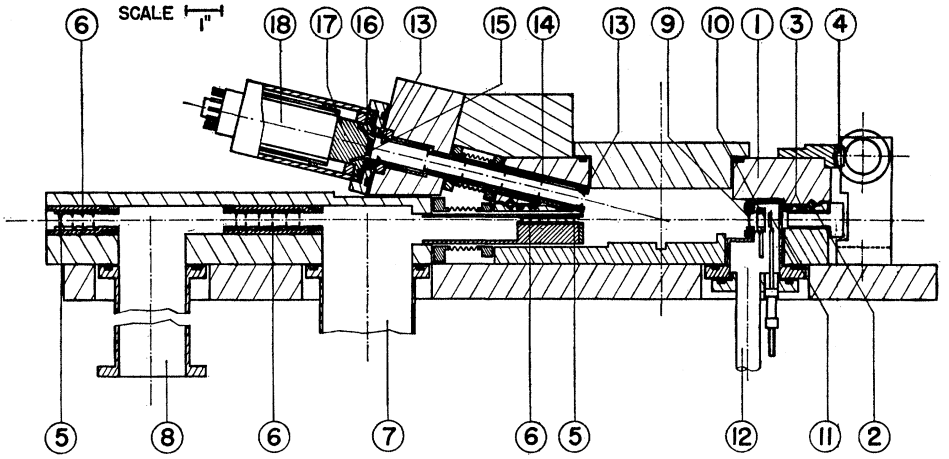

FIG. 1. Scattering chamber set at $\theta(\text{lab})=166°$ shown in cross-sectional view. (1) Rotatable top. (2) Steel balls. (3) Double O-ring seals, pumped in the interspace. (4) Worm gear drive. (5) Beam defining apertures. (6) Differential pumping impedances. (7) First differential pumping stage. (8) Second differential pumping stage. (9) Collector cup foil. (10) Suppressor electrode. (11) Beam collector. (12) To collector cup diffusion pump. (13) Counter aperture. (14) Antiscattering baffles. (15) Aluminum foil (~800 A) light shield. (16) CsI(Tl) crystal. (17) Lucite light pipe. (18) Photomultiplier—DuMont 6467.

cup body and sealed with an O-ring. This arrangement proved very convenient for changing broken foils. Suppression of secondary electrons was done by purely electrostatic means. About −2.5 kv on the suppressor electrode was found necessary.

The closeness of the collector cup to the center of the chamber caused some difficulty from particles scattered back from the tantalum disk which was initially used as a beam stop. When the counter was set at the back angle ($\theta_{\text{lab}}=166°$) the pulse-height spectrum had a large low-energy background. The background disappeared when a 1.6-mm thick graphite disk replaced the tantalum. Unfortunately, all of the He^3 back-angle data were taken under poor background conditions.

The detector consisted of a 0.5-mm thick CsI(Tl) crystal, a Lucite light pipe, and a DuMont-6467 photomultiplier. The light pipe also seals the counter system from the atmosphere. Light produced in the chamber by the beam passing through the target gas was blocked from the crystal by a 700 A aluminum foil mounted on a ring which holds the foil about 0.8 mm from the crystal. The foil was found to have a favorable effect on both pulse height and resolution. The resolution obtained with the counter was 8% for 1.7 Mev protons incident on the crystal. The resolution dropped to about 22% for 460-kev alpha particles.

The $Li^7(p,n)Be^7$ threshold measurements used for energy calibration were taken with a National Radiac NBS-1 boron-loaded zinc sulfide detector mounted on a DuMont 6467 photomultiplier and the whole assembly surrounded by paraffin.

A pressure control system was used to keep the chamber pressure constant. The basic system is the same as that used by Herring.[6,7] It consists of an oil manometer read by a cathetometer to measure the pressure and provide an error signal by means of two photocells and light sources. The error signal is amplified and used to control the influx of gas into the chamber. The system is shown schematically in Fig. 2. Stability problems were encountered in controlling the pressure due to the small volume of our chamber (about a factor of 10^{-3} smaller than the chamber used by Herring). Stability was obtained[8] by use of an integrating element in cascade in the control loop, and a gas flow control element with a faster response. A circuit diagram and operational details are in a note by Silverstein *et al.*[9] No pressure changes greater than ±0.03 mm of oil (Dow-Corning DC-704 silicone oil) occurred with the use of the above circuit.

III. EXPERIMENTAL RESULTS

A. Reduction to Cross Sections

The laboratory differential cross sections obtained from (1) were converted to center-of-mass cross sections by the usual nonrelativistic transformations.[1] The G factor was calculated by the expression[5]

$$G=G_{00}[1+\Delta_0+(\sigma'/\sigma)\Delta_1+(\sigma''/\sigma)\Delta_2+\cdots], \quad (2)$$

where

$$G_{00}=8r_1r_2^2F_1(A)/R_0hA^2, \quad (3)$$

and r_1=radius of the front aperture in cm, r_2=radius of the rear aperture in cm, R_0=distance along the center line of the aperture system from the rear aperture to the beam, and h=distance between front and rear apertures. Here $A=(1-\omega)r_2/r_1$ and $\omega=h/R_0$.

The function $F_1(A)$ is given by

$$F_1(A)=\tfrac{1}{3}[(1+A^2)E(A)-(1-A^2)K(A)], \quad (4)$$

[6] D. F. Herring, Ren Chiba, B. R. Gasten, and H. T. Richards, Phys. Rev. **112**, 1210 (1958).
[7] D. F. Herring, Ph.D. thesis, University of Wisconsin, 1957; University Microfilms, Ann Arbor, Michigan.
[8] E. A. Silverstein, Ph.D. thesis, University of Wisconsin, 1961; University Microfilms, Ann Arbor, Michigan.
[9] E. A. Silverstein, M. F. Murray, and D. F. Herring, Rev. Sci. Instr. (to be published).

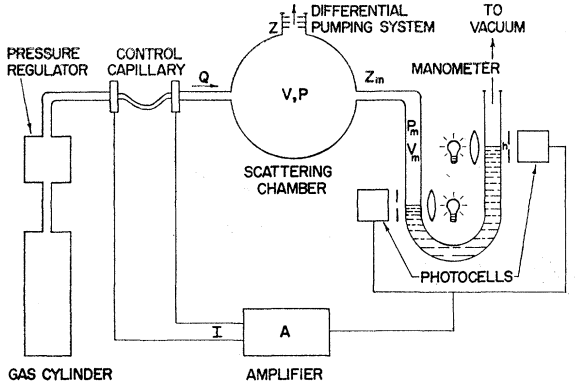

FIG. 2. Schematic of the pressure control system. The chamber of volume V is held at the pressure P by the inflow Q and the outflow Q' through the differential pumping system of impedance Z. The pressure changes in the chamber drive the manometer of volume V_m through the impedance Z_m and result in a pressure P_m which in turn drives the manometer oil resulting in a height change h. The photocells detect deviations of h from zero and the amplified error signal in the form of a heating current is applied to the control capillary, changing its impedance because of the change of gas viscosity with temperature. The gas flow Q from the constant-pressure source then changes in a direction to cancel the change in P.

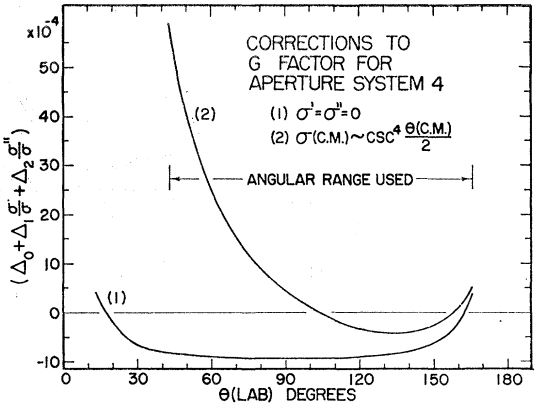

FIG. 3. G-factor corrections shown for the aperture system. The corrections are shown for a constant laboratory cross section (1) and for a Rutherford cross section (2).

where $E(A)$ and $K(A)$ are complete elliptic integrals with modulus A.

The terms in the bracket of Eq. (2) are small corrections which depend on the derivatives σ', σ'', etc. of the laboratory cross section with respect to the laboratory angle and are given in reference 5. These corrections are shown in Fig. 3 for the aperture system used for the $N^{14}(\alpha,\alpha)N^{14}$ work. For this aperture system $r_1=0.1790$ cm, $r_2=0.5509$ cm, and $G_{00}=1.0531\times10^{-3}$ cm $\pm0.3\%$. The aperture system used for most of the $O^{16}(He^3, He^3)O^{16}$ work had $r_1=0.3574$ cm, $r_2=0.5509$ cm, and $G_{00}=2.3328\times10^{-3}$ cm $\pm0.2\%$. All aperture radii are ±0.0005 cm. For all aperture sets we have $R_0=20.150\pm0.005$ cm, and $h=14.100\pm0.005$ cm.

B. Experimental Uncertainties

An estimate of the over-all accuracy of the measurements was obtained from p-p scattering data at $\theta_{c.m.}=90°$ and $E_p(\text{lab})=1.885$ Mev taken with our apparatus. Our p-p cross sections were $0.9\pm0.7\%$ higher than

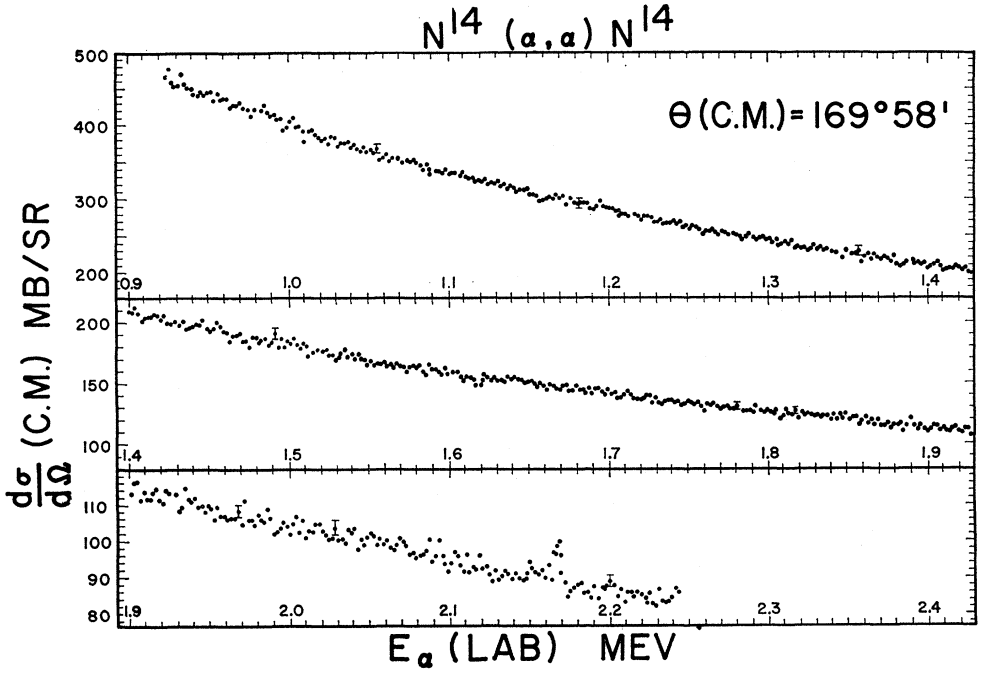

FIG. 4. Back-angle survey data showing only the 2.17-Mev resonance. Target thickness about 3 kev.

previous[10] measurements which claimed an accuracy of a few tenths percent. The above results reassure us that our measurements are free of large undetected systematic errors.

For most of the data the largest uncertainty in Y is statistical, and is indicated by bars or point size. However, for the $O^{16}(He^3,He^3)O^{16}$ data at back angle, correction for the previously mentioned low-energy tail on the pulse-height spectrum results in a systematic cross section uncertainty of about 2%. The $O^{16}(He^3,He^4)$ data were subject to additional uncertainties because of difficulties in resolving the alphas from the reaction protons.

The uncertainty in the number of target nuclei n arises from uncertainties in the manometer oil density ρ, difference in heights of the oil columns h, and target gas temperature. The oil density was known to $\pm 0.04\%$. The value of h was known to ± 0.003 cm, leading to an error ranging from 0.06% to 0.6% depending on the chamber pressure. The absolute temperature of the target gas was known to $\pm 0.1\%$. Contamination of the target gas from leaks and outgassing of parts was negligible. This was checked by taking background runs with the gas supply shut off.

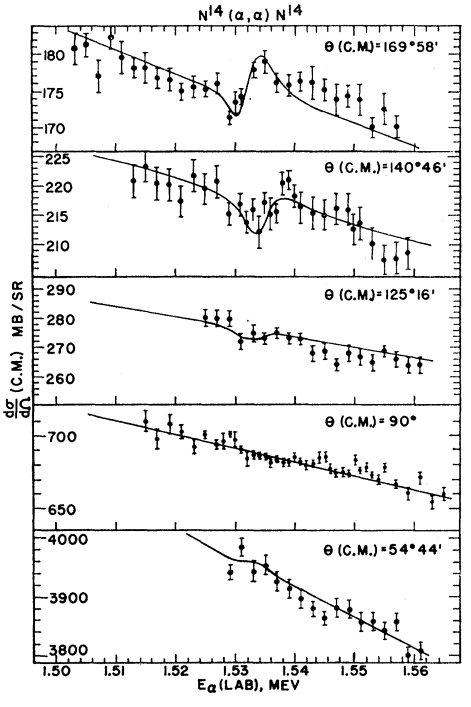

FIG. 5. $N^{14}(\alpha,\alpha)N^{14}$ differential cross sections near the 1.533-Mev resonance. Target thickness is ≤ 1.9 kev for all curves. The solid curves represent the theoretical cross section calculated for $l=1$, $J=1$, $\Gamma_\lambda=0.060$ kev, with the experimental resolution folded in. The curves were normalized to the off-resonance cross sections. This involved decreasing the theoretical cross sections by about 2%.

[10] H. R. Worthington, J. N. McGruer, and D. E. Findley, Phys. Rev. **90**, 899 (1953).

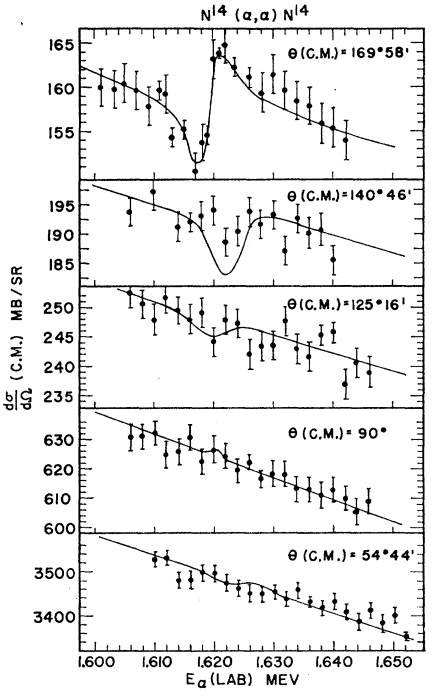

FIG. 6. $N^{14}(\alpha,\alpha)N^{14}$ differential cross sections near the 1.620-Mev resonance. Target thickness is ≤ 1.9 kev. The solid curves represent the theoretical cross section, calculated for $l=1$, $J=1$, $\Gamma_\lambda=0.2$ kev, with the experimental resolution folded in. The curves were normalized to the off-resonance cross sections, involving a decrease of about 2% in the theoretical cross sections.

Electrolytic oxygen was used for the $O^{16}(He^3,He^3)O^{16}$ work. The gas was passed through a trap cooled with a dry ice-acetone mixture before entering the pressure control capillary. A mass spectrometric gas analysis showed less than 1% nitrogen and only traces of water vapor, CO_2, etc. in the gas. For the $N^{14}(\alpha,\alpha)N^{14}$ work ordinary tank nitrogen was used with a liquid-air cooled trap. Arguments[6,8] based on the size of the $N^{14}(\alpha,\alpha)N^{14}$ elastic scattering cross section variation of the observed resonances show that these arise from N^{14} and not N^{15}.

The uncertainty in the charge collected by the integrator was $\pm 0.3\%$. A much more important uncertainty at low energies is the average charge of the bombarding He^3 or alpha particle as it emerges from the collector cup foil. The average charge on emergence from the collector cup foil was obtained from data in the review article by Allison.[11]

For the $N^{14}(\alpha,\alpha)N^{14}$ data the systematic cross-section uncertainties, where the various contributions are combined like random errors, are 1.3, 0.8, and 0.6% for $E_\alpha=1.0$, 1.6, and 2.5 Mev, respectively.

The back-angle $O^{16}(He^3,He^3)O^{16}$ data have an additional uncertainty of 2% arising from the large background subtraction. For the other angles the uncertainties are 0.9, 0.6, and 0.4% for $E_{He^3}=1.0$, 1.5, and 2.5 Mev, respectively.

[11] S. K. Allison, Revs. Modern Phys. **30**, 1137 (1958).

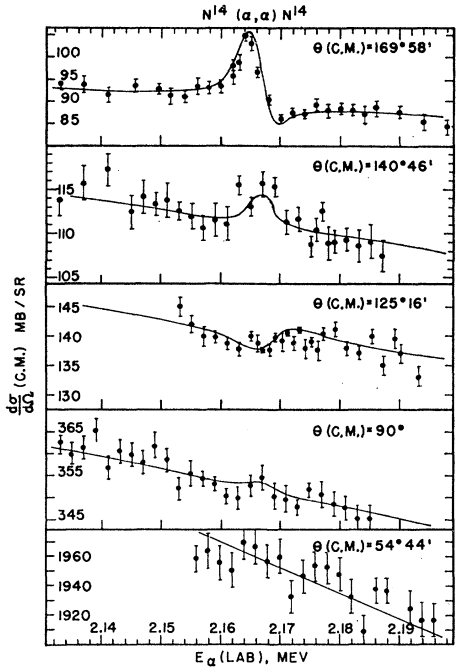

FIG. 7. $N^{14}(\alpha,\alpha)N^{14}$ differential cross sections near the 2.165-Mev resonance. Target thickness is ≤ 1.6 kev. The solid curves represent the theoretical cross section, calculated for $l=3, J=3, \Gamma_\lambda=0.2$ kev, with the experimental resolution folded in. The curves were normalized to the off-resonance cross sections, involving a decrease in theoretical cross section of about 1.5%.

The energy of the beam incident on the chamber was determined by calibrating the electrostatic analyzer by means of the $Li^7(p,n)Be^7$ threshold, taken as 1.881 ± 0.001 Mev. The energy at the center of the chamber was obtained by use of stopping power data. A fair average for our bombarding energy uncertainty for all the data is ± 2 kev.

C. Target Thickness and Experimental Resolution

Effects of experimental resolution are important for the $N^{14}(\alpha,\alpha)N^{14}$ work where the resonances are narrow. The beam energy is spread by the target thickness $(\Delta E)_T$, analyzer energy distribution $(\Delta E)_A$, energy straggling in the target gas $(\Delta E)_{str}$, and Doppler broadening from the thermal motion of the target gas $(\Delta E)_D$. (These quantities are half-widths.)

An approximate expression for the target thickness (at half-height) is

$$(\Delta E)_T = \frac{2r_1}{\omega} \times \frac{1}{\sin\theta_{lab}} \times \frac{dE}{dX}. \quad (5)$$

For all the $N^{14}(\alpha,\alpha)N^{14}$ work, the target distribution function is almost perfectly triangular. The back-angle survey was taken with a target pressure of 0.86 cm of oil and the target thickness at 2 Mev was 2.9 kev. The remainder of the $N^{14}(\alpha,\alpha)N^{14}$ data was taken with target pressures of 0.5 to 1.5 cm oil, depending on the scattering angle. At 1.5 Mev the target thickness ranged from 1.9 kev at back angle to 1.4 kev at 90°.

TABLE I. Factors contributing to experimental resolution for $N^{14}(\alpha,\alpha)N^{14}$ 1.62-Mev resonance data. We assume $(\Delta E)_{exp}^2 = (\Delta E)_A^2 + (\Delta E)_T^2 + (\Delta E)_D^2 + (\Delta E)_{str}^2$. All widths are in kev.

$\theta_{c.m.}$	h(cm)	$(\Delta E)_A$	$(\Delta E)_{str}$	$(\Delta E)_D$	$(\Delta E)_T$	$(\Delta E)_{exp}$
169°58′	0.5	0.97	3.2	0.32	1.92	3.87
140°46′	1.5	0.97	5.54	0.32	1.73	5.90
125°16′	1.5	0.97	5.54	0.32	1.46	5.82
90°	1.5	0.97	5.54	0.32	1.41	5.81
54°44′	1.23	0.97	5.02	0.32	1.68	5.39

For the $O^{16}(He^3,He^3)O^{16}$ back-angle survey the target thickness was 10 kev at 2-Mev incident energy. The remainder of the He^3 data were taken with a 5.3-kev target at $\theta(\text{lab})=90°$ for an incident energy of 2.5 Mev.

The experimental resolution function was calculated for the $N^{14}(\alpha,\alpha)N^{14}$ resonances at 1.52, 1.63, and 2.17 Mev. This function was folded in with the theoretical cross sections in an attempt to reproduce our experimental results. This function was assumed triangular in form with a half-width $(\Delta E)_{exp}$. All resolution functions contributing to $(\Delta E)_{exp}$ were approximated by triangles and half-widths were combined like random errors. Energy straggling[12] made the largest contribution to the resolution. The Doppler broadening was small and an upper estimate was used for it. Table I shows the factors

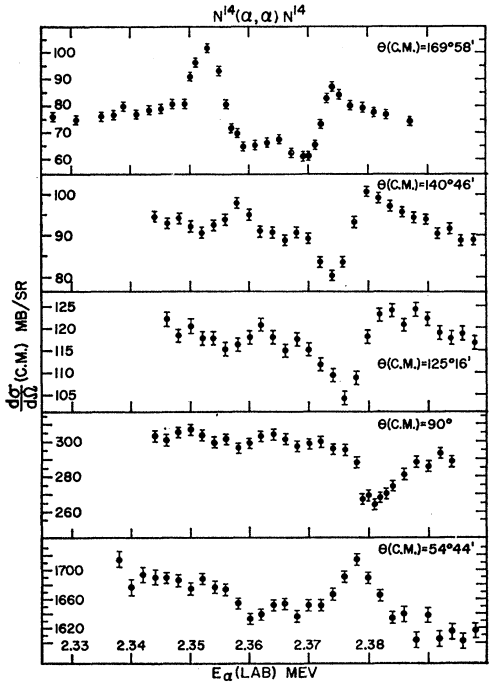

FIG. 8. $N^{14}(\alpha,\alpha)N^{14}$ differential cross sections near the 2.35- and 2.37-Mev resonances. Target thicknesses ≤ 1.5 kev.

[12] E. Segrè, *Experimental Nuclear Physics* (John Wiley & Sons, Inc., New York, 1953), Vol. 1, p. 243.

TABLE II. Summary, $N^{14}+\alpha$.

E_R(lab) Mev	J	l	Γ_λ(lab) kev	$\gamma_\lambda^2\times10^{-14}$ Mev-cm	$\gamma_\lambda^2\times\frac{2}{3}\mu a/\hbar^2$	E_λ[b] Mev excitation in F^{18}
1.533±0.003	0, 1, or 2	1	0.060[a] (For $J=1$)	3.6	0.09	5.613
1.620±0.003	0, 1, or 2	1	0.2[a] (For $J=1$)	7.2	0.17	5.681
2.165±0.003	2, 3, or 4	3	0.2[a] (For $J=3$)	7.6	0.18	6.105
2.353±0.005	2, 3, or 4	3	~1 (For $J=3$)	~20	~0.5	6.251
2.375±0.005	1	0	~2	~0.9	~0.02	6.269

[a] Γ_λ extracted from data depends on J value assumed. (A smaller/larger J would permit a larger/smaller Γ_λ. These values are probably accurate to ~30%. The same remarks apply to γ_λ^2 and to $\gamma_\lambda^2\times\frac{2}{3}(\mu a/\hbar^2)$.
[b] Calculated using 4.421 as the energy difference between $N^{14}+\alpha$ and the ground state of F^{18}.

contributing to the experimental resolution for the 1.62-Mev resonance.

The experimental results are shown in Figs. 4–12.

IV. ANALYSIS AND DISCUSSION

A. $N^{14}(\alpha,\alpha)N^{14}$ Data

The formalism used in the analysis of the data is the Wigner-Eisenbud one-level formula for the case of the elastic scattering of a spin-zero projectile by a nucleus of spin one. The formalism and notation used here is the same as that used by Herring,[7,13] and by Galonsky and McEllistrem[14] and is not reproduced here. Only one l value is assumed to contribute to a particular compound nucleus state. There was no evidence in our work for the incorrectness of this assumption which was made mainly for the sake of simplicity of analysis. The rapid variation of the penetrability at the low energies used here works in favor of the assumption. For instance, at $E_\alpha=1.53$ Mev, the Wigner limit on reduced width gives (for $a_\alpha=4.8\times10^{-13}$ cm) an observed width $\Gamma_\lambda\leq0.71$ kev for $l=1$. In order to conserve parity, the next l value permitted is $l=3$. However, for $l=3$, $\Gamma_\lambda\leq0.016$ kev. This factor of ≈45 in maximum observed widths can be said to strongly discriminate against, but not forbid, the higher l value.

The theoretical cross sections obtained by means of the above formalism were folded in with the experimental resolution to obtain the curves shown below in Figs. 5–7. The values of Γ_λ and resonant energy E_R were adjusted to give the best fit to the data for the l value selected. The l value was determined by the shape of the resonances and their behavior at the various angles. The theoretical absolute cross sections thus obtained were then normalized to the off-resonant experimental cross sections. This involved decreasing the theoretical cross sections by ≈2% near 1.53 and 1.62 Mev, and by ≈1.5% near 2.17 Mev. These decreases are consistent with our assigned systematic errors. Hard-sphere phase shifts were not included in the calculation as they are very small at these energies.

The back-angle survey shown in Fig. 4 shows only the 2.17-Mev resonance. The later data (Figs. 5–7) in this energy region were taken with thinner targets, and are discussed below.

1. Resonance at 1.533 Mev (Fig. 5). The behavior of this resonance is well accounted for by an assignment of $l=1$ to the incoming α particles and a laboratory width of $\Gamma_\lambda\approx60$ ev, which is 10% of the Wigner limit. The solid curves were obtained by assuming $J=1$ and $E_R=1.533$ Mev. Different J values change the peak height of the theoretical cross-section curve, but the experimental resolution is so large compared to the true resonance width that we cannot distinguish between $J=0$, 1, or 2. For $J=0$ the data could be fit by a larger Γ_λ, for $J=2$ a smaller Γ_λ would suffice. The shape of the cross-section curve quite well determines the l value to be $l=1$ even though J cannot be determined. Penetrability arguments show that we need only consider l values up to $l=3$.

2. Resonance at 1.620 Mev (Fig. 6). The theoretical fit is for $l=1$, $J=1$, $\Gamma_\lambda=200$ ev, $E_R=1.620$ Mev. This value of Γ_λ is 17% of the Wigner limit. Again, $J=0$ or 2 are not excluded by the data and imply a larger or smaller value of Γ_λ, respectively. We can assume $l\leq3$ since the Wigner limit on the reduced width gives $\Gamma_\lambda\leq26$ ev for $l=3$. However $l=0$ or 2 gives the wrong shape. The fit at $\theta_{c.m.}=140°46'$ is not good, but not bad enough to preclude the assignment of $l=1$. If the resonance were $l=3$, the theoretical cross-section curve would be much flatter at 140°46′, which would be more in agreement with the data. However, such behavior would imply that the resonance was mainly $l=3$, and such a resonance would look qualitatively like the one shown in Fig. 7 and hence would not fit our data.

3. Resonance at 2.165 Mev (Fig. 7). The assignment of $l=3$ to the α particles forming this resonance gives a good fit to the shape of the cross-section curves at all angles studied. The solid curves assume $l=3$, $J=3$, $E_R=2.165$ Mev, and $\Gamma_\lambda=200$ ev, corresponding to

[13] D. F. Herring, Phys. Rev. **112**, 1217 (1958).
[14] A. Galonsky and M. T. McEllistrem, Phys. Rev. **98**, 590 (1955).

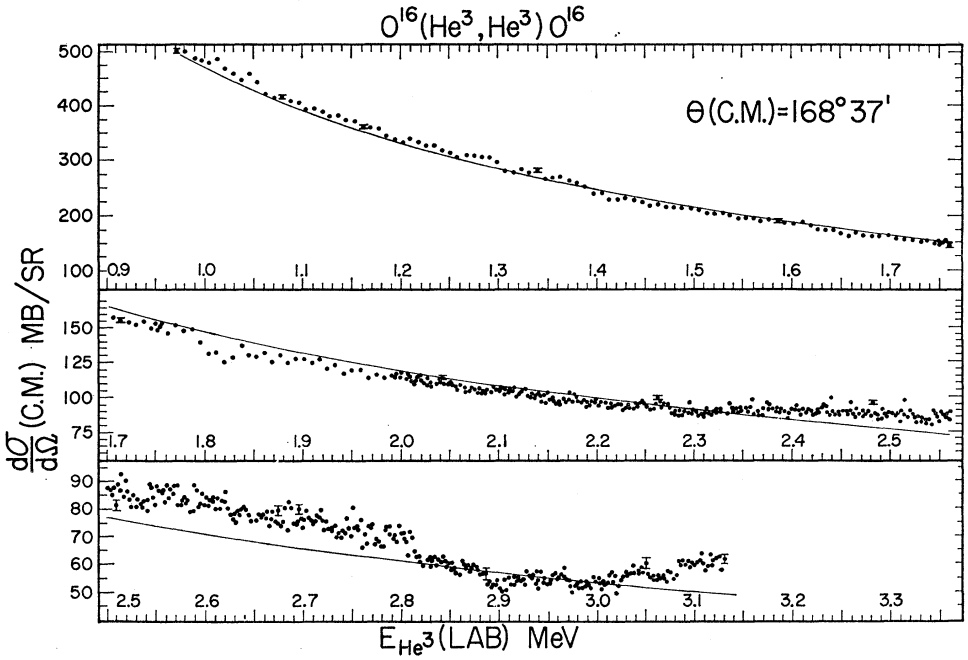

FIG. 9. $O^{16}(He^3,He^3)O^{16}$ back-angle differential cross section. The solid curve is the Rutherford cross section. The large scatter of the data points at the back angle results from uncertainties in subtraction of a background tail of the elastic peak.

$\approx 30\%$ of the Wigner limit. Again, by use of a different Γ_λ one can still fit the data with $J=2$ or 4.

4. Resonances at 2.35 and 2.37 Mev. Figure 8 shows our data on the 2.35- and 2.37-Mev resonances. These data were taken mainly to check Herring's[13] tentative assignment of $l=3$ for the 2.35-Mev resonance and were taken with thinner targets than those used in his work. From the behavior at all angles of this resonance an assignment of $l=3$ is indicated, confirming Herring's assignment. This can be seen by comparing the shape of the $l=3$ resonance at 2.165 Mev in Fig. 7 with the first resonance in Fig. 8. (The shapes will be very similar since the energies are close together.) The possibility of $l=2$, mentioned by Herring, is eliminated by the back-angle data, since an $l=2$ resonance would be an almost pure dip. Our data on the 2.37-Mev resonance are consistent with Herring's assignments of $l=0$.

The $N^{14}(\alpha,\alpha)N^{14}$ results are summarized in Table II. The positions of the 1.533- and 1.620-Mev levels agree well with those found from $N^{14}(\alpha,\gamma)F^{18}$ work by Price[2] and Phillips.[3] The assignment of $J=1^-$ for the 1.525-Mev level by Almqvist *et al.*[15] is consistent with our

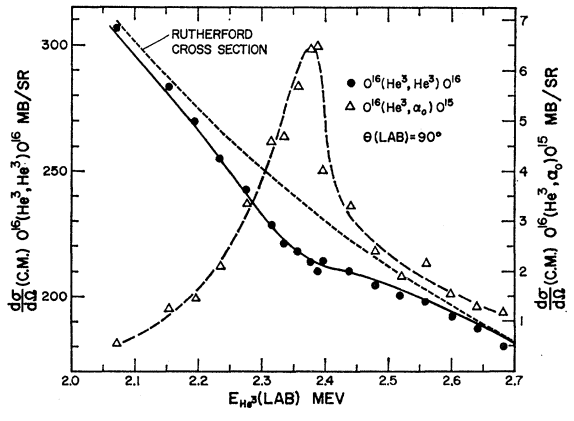

FIG. 10. $O^{16}(He^3,He^3)O^{16}$ and $O^{16}(He^3,\alpha)O^{15}$ data taken simultaneously at θ(lab)$=90°$. θ(lab) of 90° corresponds to $\theta_{c.m.}=100°52'$ for the elastic scattering.

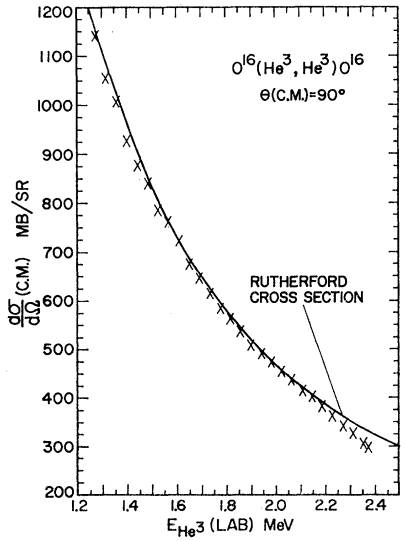

FIG. 11. $O^{16}(He^3,He^3)O^{16}$ cross sections measured at θ(c.m.)$=90°$.

[15] E. Almqvist, D. A. Bromley, and J. A. Kuehner, Bull. Am. Phys. Soc. 3, 27 (1958).

assignment of $l=1$, $J=0$, 1, or 2. The suggested assignment[16] of $J=1^-$ for the 1.620-Mev level is also consistent with our assignment of $l=1$, $J=0$, 1, or 2. The 2.165-Mev level was not seen by previous γ-ray work, but was seen by Hinds and Middleton[4] in the $F^{19}(He^3,\alpha)F^{18}$ reaction. Figure 13 compares levels in F^{18} found by them with levels found in the present work. The levels at 5.785 and 6.137 Mev excitation in F^{18} were not seen in our work and hence their $\Gamma_\alpha \ll 1$ kev. The assignment of $T=1$ to the 2.353-Mev level (6.251-Mev excitation in F^{18}) by Warburton[16] is contradicted by our data. Since the Γ_α of this level is near the Wigner limit and both N^{14} and the alpha are $T=0$, only $T=0$ is permitted for the F^{18} level if isobaric spin is a useful quantum number.

B. $O^{16}+He^3$ Data

The back-angle elastic scattering survey is shown in Fig. 9. Fig. 10 shows our 90° (lab) data for both elastic scattering and the (He^3,α) reaction. Figure 11 shows the elastic scattering data at θ(c.m.)$=90°$. The broad resonance structure in the (He^3,α) reaction has been seen earlier by Bromley *et al.*[17] In view of the previously mentioned background difficulties for the back-angle elastic He^3 data no theoretical fit was made; however, the smallness of the excursions from Rutherford is not unreasonable. We see evidence of the start of another resonance where the cross section begins to rise above 2.9 Mev.

Bromley *et al.* have interpreted the resonance structure in the $O^{16}(He^3,He^4)O^{15}$ ground-state alphas as arising from interference between two levels in Ne^{19} of the same parity. Our elastic He^3 data show destructive interference with Rutherford scattering near θ(c.m.) $=90°$ (Figs. 10–12). Therefore an even l-value assignment is required for the He^3 particles forming the compound states in Ne^{19}, and hence the parity of this two-level combination is even.

The Wigner-Eisenbud one-level formula for the case of the scattering of particles of spin $\frac{1}{2}$ by target nuclei of spin 0 was used to interpret our data and compare them with Bromley's. The formalism and notation is the same as that used by Olness *et al.*[18] and is not reproduced here. For an interaction radius we took $1.45(16^{\frac{1}{3}}+3^{\frac{1}{3}})\times10^{-13}$ cm$=5.73\times10^{-13}$ cm.

The solid curve in Fig. 10 shows the theoretical cross section calculated for a single level with $l=0$, $J=\frac{1}{2}^+$, $\Gamma_\lambda=300$ kev, $E_R=2.36$ Mev, and the ratio of elastic width to total width $\Gamma_{\lambda e}/\Gamma_\lambda=0.11$. These later values are reasonably close to those of reference 17. Here E_R is the resonant energy, taken as the energy for which the resonant phase shift is 90°. $E_R=E_\lambda+\Delta_\lambda$, where Δ_λ is

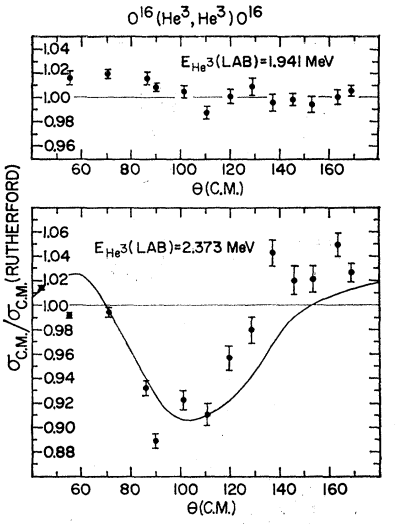

FIG. 12. $O^{16}(He^3,He^3)O^{16}$ angular distributions at E_{He^3} (lab) $=1.941$ and 2.373 Mev. The ratio of differential cross section to the Rutherford cross section is plotted. The solid curve at 2.373 Mev represents the theoretical angular distribution calculated for the resonant parameters $J=\frac{1}{2}^+$, $\Gamma_\lambda=300$ kev, $E_R=2.36$ Mev, and $\Gamma_{\lambda e}/\Gamma_\lambda=0.11$.

the level shift defined in reference 18. The level shift Δ_λ and Γ_λ were assumed energy independent. The value of Δ_λ depends on the l values of all the proton partial widths [widths for the reaction $O^{16}(He^3,p)F^{18}$ to various states of F^{18}]. These were unknown, but since $\sum\Gamma_p \approx 170$ kev,[17] a rough estimate shows that the level shift could be around 100 kev. The other resonance does not make a contribution to the curve in Fig. 10 if we take Bromley's value of $\Gamma_{\lambda e}/\Gamma_\lambda=0.01$ since the resonant scattering amplitude is multiplied by $\Gamma_{\lambda e}/\Gamma_\lambda$. The fit of the theoretical curve in Fig. 10 to the data is satisfactory in view of our neglect of the energy variation of Γ_λ, Δ_λ, and effects arising from higher resonances. The angular distribution at 2.373 Mev in Fig. 12 was calculated assuming the above values for the broad resonance. The narrow resonance would not be expected to show up in the angular distribution. We see no evidence in our

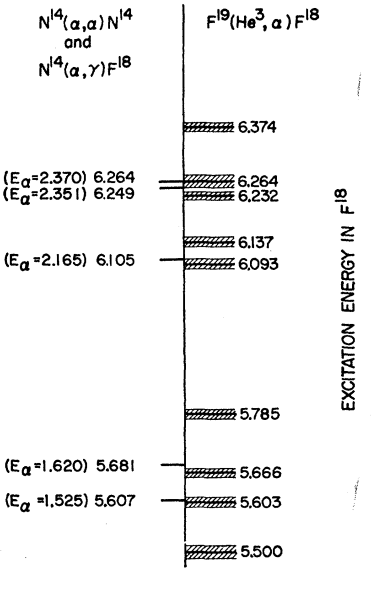

FIG. 13. Comparison of the levels found by Hinds and Middleton (the cross-hatching represents their quoted uncertainties) from the $F^{19}(He^3,\alpha)F^{18}$ reaction with those found from our $N^{14}+\alpha$ elastic scattering data.

[16] E. K. Warburton, Phys. Rev. **113**, 595 (1959).
[17] D. A. Bromley, J. A. Kuehner, and F. Almqvist, Nuclear Phys. **13**, 1 (1959).
[18] J. W. Olness, W. Haeberli, and H. W. Lewis, Phys. Rev. **112**, 1705 (1958).

TABLE III. Summary, $O^{16}+He^3$.

E_R(lab) (Mev)	Excitation[a] in Ne^{19} (Mev)	Γ_λ(c.m.) (kev) Total width	$\Gamma_{\lambda e}$ Elastic He^3 width (kev)	$\gamma_{\lambda e}^2\times10^{-14}$ (Mev-cm)	$\gamma_{\lambda e}^2\times\frac{2}{3}\mu a/\hbar^2$	l	J	π	Γ_{He^4}[c] (kev)	Γ_p[c] proton widths (kev)
2.360	10.405	300	33	10	0.233	0	$\frac{1}{2}$	+	135	170
2.425[b]	10.457	45[b]	0.45[b]	0.8[b]	0.019[b]	2[b]	$\frac{5}{2}$[b]	+	22.3[b]	22.3[b]

[a] $O^{16}+He^3$ is taken at 8.419 Mev in Ne^{19}.
[b] These values were not determined from our data, but are from Bromley *et al.*, reference 17. They are not inconsistent with our work.
[c] Values from Bromley *et al.*, reference 17.

elastic scattering data for the existence of the narrow 2.42-Mev level.[17]

The magnitude of the dip in the angular distribution data at 2.373 Mev determines the value of $\Gamma_{\lambda e}/\Gamma_\lambda$ for the broad resonance to be 0.11. [This value is also necessary for a fit to the excitation function at θ(c.m.) $=100°52'$ (Fig. 10).] The peak which would be expected at θ(c.m.)$\approx60°$ (Fig. 12) is not present in our data. Such a peak must occur very near this angle and with very nearly the magnitude shown on the theoretical curve for a pure S-wave resonance. The absence of this peak is attributed to interference from higher levels. In order to make the angular distribution fit the data better at back angles (i.e., to make σ/σ_R at $180°\approx1.04$) we would require a large change (around 10°) in the resonance phase shift. This would ruin the fit to the excitation function as it would require a downward change of about 40 kev in the resonant energy. We can conclude that the experimental points are high from either background effects or effects of higher resonances.

The results of the $O^{16}+He^3$ work are summarized in Table III.